

Liquid injection in confined co-flow: Application to portal vein embolization by glue injection

M.-C. Sandulache, P. Paullier, R. Bouzerar, T. Yzet, O. Balédent et al.

Citation: *Phys. Fluids* **24**, 081902 (2012); doi: 10.1063/1.4740059

View online: <http://dx.doi.org/10.1063/1.4740059>

View Table of Contents: <http://pof.aip.org/resource/1/PHFLE6/v24/i8>

Published by the [American Institute of Physics](http://www.aip.org).

Related Articles

Transport of particles by magnetic forces and cellular blood flow in a model microvessel
Phys. Fluids **24**, 051904 (2012)

Reducing the data: Analysis of the role of vascular geometry on blood flow patterns in curved vessels
Phys. Fluids **24**, 031902 (2012)

Dynamics of microcapsules in oscillating shear flow
Phys. Fluids **23**, 111901 (2011)

Pair collisions of fluid-filled elastic capsules in shear flow: Effects of membrane properties and polymer additives
Phys. Fluids **22**, 123103 (2010)

Natural constructal emergence of vascular design with turbulent flow
J. Appl. Phys. **107**, 114901 (2010)

Additional information on Phys. Fluids

Journal Homepage: <http://pof.aip.org/>

Journal Information: http://pof.aip.org/about/about_the_journal

Top downloads: http://pof.aip.org/features/most_downloaded

Information for Authors: <http://pof.aip.org/authors>

ADVERTISEMENT



**Running in Circles Looking
for the Best Science Job?**

Search hundreds of exciting
new jobs each month!

<http://careers.physicstoday.org/jobs>

physicstodayJOBS



Liquid injection in confined co-flow: Application to portal vein embolization by glue injection

M.-C. Sandulache,¹ P. Paullier,¹ R. Bouzerar,² T. Yzet,³ O. Balédent,² and A.-V. Salsac^{1,a)}

¹Laboratoire Biomécanique et Bioingénierie (UMR CNRS 7338), Université de Technologie de Compiègne, BP 20529, 60205 Compiègne, France

²Département d'Imagerie Clinique et Biophysique, CHU Amiens – Université de Picardie Jules Verne, Place Victor Pauchet, 80054 Amiens cedex 1, France

³Département de Radiologie, CHU Amiens, Place Victor Pauchet, 80054 Amiens cedex 1, France

(Received 30 September 2011; accepted 16 July 2012; published online 16 August 2012)

Drop formation in liquid-liquid systems has received considerable attention over the last century owing to its many industrial applications. More recent applications may be found in the field of endovascular/percutaneous treatments. The present study focuses on portal vein embolization (PVE), which consists in the blockage of part of the portal trunk through the injection of surgical glue. The short-time injection is dominated by fluid dynamic effects: the influence of polymerization is secondary owing to the presence of ethiodized oil in the injected mixture. If the mechanism of liquid injection is well understood for injections in unconfined fluids at rest, fewer studies have so far considered the case of outer liquids flowing in confined environments. The objective is therefore to conduct a large range parametric study of liquid injections in confined co-flows. An experimental setup has been designed to simulate *in vitro* the injection in an immiscible liquid flowing in a cylindrical tube. The transition from the dripping to the jetting regimes is found to be independent of confinement, but to depend on the ratio of the inertial forces of the injected liquid to the surface tension, i.e., the Weber number of the inner flow We_i . The confinement, however, has an influence on the drop size in the dripping regime. Its influence diminishes in the first phase of the jetting regime, as the drop size largely decreases. In the fully established jetting regime, the drop size is finally only a function of the ejection tube diameter. To predict the size of the drops in the dripping regime, we have developed a semiempirical model that takes into account the effects of both the tube confinement and outer flow. It will help the interventional radiologists predict the drop size depending on the geometrical and velocimetric conditions at the site of embolization. All these results can then serve as a base to optimize the PVE technique during clinical practice. © 2012 American Institute of Physics. [<http://dx.doi.org/10.1063/1.4740059>]

I. INTRODUCTION

Embolization by glue injection is a therapeutic treatment technique used to block the blood flow to targeted sites. It consists in injecting a surgical glue locally into the blood stream, the polymerization being initiated by the blood ions.¹ Glue embolization has been reported to be the indicated treatment for gastrointestinal bleeding² and arteriovenous malformations,³ and to be more effective than other treatment techniques (e.g., particulate embolization).⁴ Another application of glue embolization concerns patients suffering from malignant liver tumors, who need to undergo partial liver ablation (hepatectomy). When the volume of the future liver remnant (FLR) is insufficient, patients

^{a)}Electronic mail: a.salsac@utc.fr. URL: www.utc.fr/bmbi.

present risks of postoperative hepatic failure.^{5–8} Preoperative portal vein embolization (PVE) is then performed ahead of the surgery in order to occlude the venous branches of the malignant part of the liver. It induces the FLR hypertrophy and therefore enables the ablation procedure after a couple of weeks, when the FLR volume is no longer sub-critical.⁹

Portal vein embolization is typically performed percutaneously: a copolymer glue with a cyanoacrylate base is injected through a catheter, after being mixed with a radio-opaque iodized oil. If the reaction time of the glue itself is very short (initiation time: 1–2 s, time for complete polymerization: 60–90 s),¹⁰ it is considerably increased in the presence of the ethiodized oil, the initiation time increasing to 5–20 s depending on the concentration in oil.

The clinical practice of glue embolization is currently based mostly on empirical knowledge, as indicated by the guidelines provided to the interventional radiologists.¹¹ Very few studies have modeled the process. White and Smith¹² and White¹³ have, for instance, considered the two-phase flow that exists in a bifurcating channel far from the site of injection. They have assumed the fluid mimicking the glue mixture to occupy most of the vessel cross section, the blood flow being confined to a very thin boundary layer. No other study has investigated the embolization of vessel *in vitro* or *in silico* and explored the becoming of the glue once ejected. The objective of the present study is thus to provide a better understanding of the physical phenomena controlling the injection and convection of the embolic liquid in a confined blood flow. It would help reduce the risks of comorbidity and morbidity associated with the treatment. Since embolizing injections last about 30 s in clinical practice, polymerization effects have little time to take place during the injection. We will therefore neglect the kinetics of polymerization as a first approximation and study the dynamics of the injection in a co-flowing immiscible liquid within a cylindrical tube.

When a liquid is injected in an immiscible outer liquid, two regimes of ejection exist. At low injection velocities, drops form at the tip of the injection tube, grow and eventually detach from the tube: it is the dripping regime. A transition to the jetting regime occurs at higher injection velocities: the inner fluid exits the tube as a jet that breaks up downstream into small drops as a consequence of the Rayleigh-Plateau instability.^{14,15}

A. Dripping regime

Drop formation in liquid-liquid systems has received considerable attention over the last century owing to its many industrial applications in chemical engineering (emulsifications, extractions, chemical reactions, etc.), ink jet printing, production of spherical particles, beads, microcapsules, etc.^{16,17} Studies have tried to explain the mechanism accounting for the formation of the drop and predict its size. Many studies have considered the formation of droplets in *unconfined* environments with an outer fluid at rest. Early experimental studies^{18,19} have focused on the dripping regime and investigated the effects of the parameters controlling the drop size. They showed that the size of the forming drops increases with the injection diameter, interfacial tension, and viscosity of the outer fluid or when decreasing the injection velocity and density difference between the two fluids. It has also been observed that the drop viscosity has no influence on its final size. If one translates these results in terms of non-dimensional numbers, it indicates that, besides the inner-to-outer viscosity ratio η , the drop formation is mainly influenced by the capillary number Ca , ratio of viscous to surface tension forces and by the Weber number We , ratio of inertial to surface tension forces. The other non-dimensional numbers that play an important role are the Bond number Bo , which compares gravitational to surface tension forces and the Reynolds number Re , which compares inertial to viscous forces.

Formation of drops in an external quiescent liquid has since then been investigated extensively both experimentally and numerically. Numerically, two main approaches are used to simulate multiphase flows:^{17,20} interface tracking methods and interface-capturing methods. Interface tracking methods include boundary integral,²¹ finite element,²² and immerse-boundary methods.²³ They rely on the meshing of the different fluid domains and of their interphases: the latter can therefore be tracked with a very high accuracy. In interface-capturing methods, however, the interface has no physical existence: the location of the discontinuity in fluid properties is itself a result of the simulation. The surface tension force is then imposed as a volume force distributed over a thin

region around the interface. Among the different numerical methods that exist, one can cite the volume-of-fluid,^{24,25} phase-field,²⁶ and lattice-Boltzmann methods.²⁷

The first correlations for the prediction of drop size during dripping have been developed in the 1950s for an external fluid at rest. For instance, Hayworth's model¹⁸ is based on the balance between the buoyancy force, kinetic force, drag force, and interfacial force that act on the drop prior to its detachment from the tip of the injection tube. Hayworth¹⁸ found a good agreement between his correlations and experimental results in the limited range of liquid properties and nozzle sizes that he tested. Later studies^{28–31} developed semi-empirical models that take into account the two stages of the drop formation process in the dripping regime. The first stage is characterized by a pure static growth of the drop that ends with the loss of the force equilibrium. The second stage corresponds to the necking and subsequent drop detachment from the nozzle. The final volume of the drop encompasses the static volume from the first stage and an additional volume that enters the drop during the necking process. The model of Scheele and Meister²⁹ appears to be the best compromise between accuracy and simplicity of use; it predicts the drop volume with a 15% accuracy for low viscosity liquid-liquid systems. The calculation of the drop diameter becomes iterative, when the outer phase viscosity exceeds 10 mPa s, as the drag term can no longer be neglected. Future studies have shown that the correlation should be used with caution outside the range of prescribed parameter values, as its accuracy fails rapidly.

The influence of an *external flow* on the drop formation has been considered more recently.^{32–34} In the last two decades, the development of microfluidic devices has led to a recrudescence of interest on both experimental^{35–40} and numerical^{41,42} grounds. But among all the studies that have considered the injection under co-flow, very few of them have looked at the influence of *confinement*. Only Zhang³³ studied its consequences on the shape of the drop just prior and after detachment. The only theoretical model of a drop exposed to an unbounded external flow has been proposed by Umbanhowar *et al.*⁴³ It is only valid for Stokes flow conditions and requires the use of a fitting parameter. No existing model takes into account the influence of confinement.

B. Jetting regime

Great attention has equally been paid to the drop formation in the jetting regime both experimentally and numerically, e.g., Refs. 24, 44, 45, but only for an outer fluid at rest. Tyler⁴⁶ was the first to apply Rayleigh's linear stability analysis¹⁵ to predict the drop size. He postulated that the drop generated from a cylindrical jet has the same volume as the portion of the jet of length equal to the disturbance wavelength on the jet surface. But this simple model is only valid when applied to jets into air.⁴⁶ The first study of the breakup of a liquid jet into another immiscible liquid was performed by Tomotika.⁴⁷ He calculated the most unstable wavenumber for different viscosity ratios. Many theoretical and experimental studies used Tomotika's theory to predict the jet length and the drop size when a jet is injected into an immiscible quiescent liquid.^{24,48–52}

C. Dripping-to-jetting transition

Previous studies have finally shed some light on the mechanism underlying the existence of two distinct regimes. Stability studies have concluded that the transition from drop generation to jet formation is, in general, due to a transition from absolute to convective instability,^{53,54} even though cylindrical jets may occasionally break up due to an absolute instability.⁵⁵ Phenomenological studies have provided a clear understanding of the transition between dripping to jetting in the case of water injected in air.^{56–58} However, the results are not directly applicable to glue embolization: being a liquid-liquid system, its inner and outer flow fields are largely influenced by the viscosity ratio.

Cramer *et al.*⁵⁹ performed an experimental study of the transition for liquid-in-liquid systems. They concluded that the dripping-to-jetting transition is favored by any parameter that enhances the drag force of the outer phase and increases the momentum of the dispersed inner phase. A more universal framework was provided by Utada *et al.*⁶⁰ based on microfluidic injections in a liquid co-flowing in a millimetric tube (no confinement effect). They identified the non-dimensional numbers that govern the transition. They showed the existence of two different jetting regimes: (i) a transition

to widening jets takes place when the inertial forces of the inner fluid overcome the interfacial tension; (ii) a transition to narrowing jets occurs when the interfacial tension is overcome by the viscous drag exerted by the outer fluid on the liquid interface. They concluded that the condition for the formation of a widening jet is a Weber number of the inner fluid $We_i \gtrsim 1$. In the case of a narrowing jet, the condition is a capillary number of the outer fluid $Ca_o \gtrsim 1$. This dripping-to-jetting criterion was completed by Castro-Hernandez *et al.*,⁶¹ who added the influence of the Reynolds number. Their experimental results showed that the transition to widening jets occurs for $We_i \gtrsim 1$ only when the Reynolds number of the inner fluid $Re_i > 1$. No influence of the Reynolds number is, however, found on the transition to narrowing jets.

In conclusion, one can notice that despite the large body of experimental, numerical, and theoretical studies on liquid-in-liquid injections, the influence of confinement has received little attention. Existing results cannot be directly applied to explain the injection phenomena that are encountered during PVE. There is therefore the need to study the injection simulating the same range of non-dimensional parameters that are encountered during PVE *in vivo*. Hence, the objectives of the present study are twofold: (i) to conduct an *in vitro* study of the co-flow injection in a millimetric-sized confined environment; (ii) to develop a corresponding theoretical model to predict the droplet size in the dripping regime. In Sec. II, we describe the experimental setup used to simulate glue embolization *in vitro*, the liquids used as fluid-models and the data acquisition techniques. In Sec. III, we show the influence of confinement on the inner fluid flow topology and drop size. We then present in Sec. IV a new theoretical model that predicts the drop size in the dripping regime for confined outer flows. Finally, in Sec. V, we analyze the results and discuss their implication for glue embolization in clinical practice.

II. MATERIAL AND METHODS

A. Experimental setup

An experimental setup (Figure 1) has been designed to create and visualize the confined co-flow of two immiscible fluids. The inner fluid is injected through a capillary tube of inner diameter d_i (Figure 2). It is placed concentrically in a straight cylindrical glass tube of inner diameter d_o , in which the outer fluid flows steadily. The tip of the capillary tube is placed $15 \times d_o$ from the glass tube entrance to ensure that the outer flow is fully developed at the location of injection when the inner fluid is ejected. The following tube sizes are tested: $d_i = 0.5$ mm and 1.6 mm; $d_o = 7$ mm

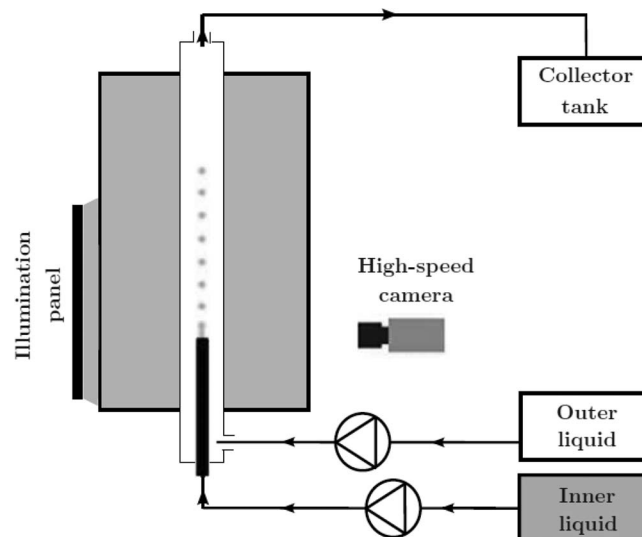


FIG. 1. Schematic view of the experimental setup.

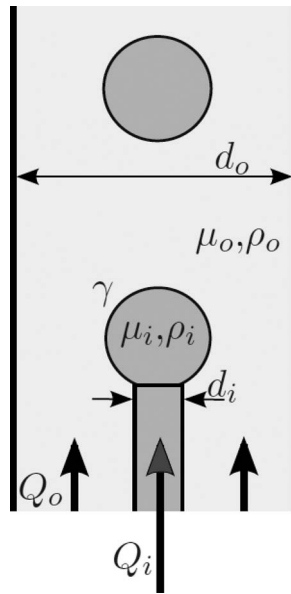


FIG. 2. Physical and geometrical quantities controlling the liquid-in-liquid confined injection.

and 10 mm. The glass tube is placed in a transparent tank filled with water to eliminate the visual distortions caused by the tube curvature.

A continuous-flow gear pump (Ismatec MCP-Z with head Z-130) generates the outer fluid flow with flow rate Q_o (Figures 1 and 2). The inner fluid flow is generated at flow rate Q_i by a syringe pump (KDS 200P, kdScientific). Both fluids flow in the anti-gravitational direction. In order to visualize the injection, we use a high-speed imaging system (Photron Fastcam SA3). The camera captures 2000 frames/s at its maximum resolution (1024×1024 pixels); its shutter can be adjusted from 16.7 ms to $2 \mu\text{s}$. A flat panel with optical fibers (Schott-Fostec, LLC) provides a back illumination. The experiment is conducted at room temperature and all the recordings are performed at least 10 min after the onset of the outer flow, to ascertain that it is fully established and stationary.

The size d_d of the forming drops and their formation time t_d are evaluated from the recorded image sequences. The drop size is measured at a distance of ~ 40 mm from the tip of the capillary tube, where the drop has an almost stationary spheroidal shape. The major and minor axes of the spheroid are measured manually on the images; the reference length used for calibration is the outer diameter of the external glass tube. The equivalent diameter \bar{d}_d of the drop is the diameter of the sphere having the same volume as the spheroid. For each set of experimental conditions, we have calculated the mean drop size \bar{d}_d , averaging over 50 consecutive drops. The main source of error comes from the determination of the drop minor axis along the vertical direction: the drop contour tends to be less visible on the images at the top and bottom of the drop. We estimate that an error of ± 4 pixels is made in the determination of the minor axis, the size of a pixel being about 0.08 mm. For the major axis of the drop, the error comes down to ± 2 pixels, which corresponds to twice the contour thickness. Consequently, the error in the measurement of \bar{d}_d is about $\pm 7\%$. An additional source of error comes from the fact that the satellite drops are not taken into account in the calculation of the mean drop size, when their formation is occasional and their equivalent diameter inferior to $0.3 \times \bar{d}_d$. But, in such cases, we have never observed more than 8 satellite drops for every 100 primary drops. The error is therefore much smaller than 1%.

Deionized water is used as the outer liquid and a silicon oil (DC200, Sigma-Aldrich 85411) as the inner liquid. The physical properties of the two liquids have been measured at room temperature $T = 21^\circ \pm 1^\circ\text{C}$. The fluid viscosity μ is measured using a rheometer (RheoStress 1, Thermo Haake) with a cone and plate cell varying the shear rate from 50 s^{-1} to 1500 s^{-1} . Both liquids exhibit a Newtonian behavior. The measured values of viscosity are indicated in Table I, along with the values of the density ρ and the interfacial tension γ . The density is measured with an oscillating

TABLE I. Physical properties of the fluids used *in vitro*. The interfacial tension γ has been measured between the silicon oil and deionized water.

	μ_k ($\times 10^{-3}$ Pa s)	ρ_k (kg m^{-3})	γ ($\times 10^{-3}$ N/m)
Silicon oil ($k = i$)	10	937	32
Deionized water ($k = o$)	1.003	998	

U-tube densimeter (Anton Paar DMA 45). The interfacial tension is determined using a pendant drop analysis system (Drop Shape Analysis System DSA10, Kruss).

B. Dimensionless numbers

Based on the physical and geometrical quantities defined in Figure 2, one can provide the following definitions for the dimensionless numbers defined in the Introduction (Sec. I). The effect of confinement is measured by the size ratio d_o/d_i . The viscosity ratio is $\eta = \mu_i/\mu_o$. The inner and outer Reynolds numbers are $Re_k = 4\rho_k Q_k/\pi d_k \mu_k$ ($k = i, o$), the index k referring either to the inner fluid ($k = i$) or the outer fluid ($k = o$). The Weber number of the inner fluid is $We_i = 16\rho_i Q_i^2/\pi^2 d_i^3 \gamma$. The capillary number of the outer fluid is $Ca_o = 4\mu_o Q_o/\pi d_o^2 \gamma$. The Bond number is $Bo = (\rho_o - \rho_i) d_i^2 g/\gamma$, where g is the gravity. We have varied the flow rates and characteristic lengths of both the inner and outer fluid flows. The values of the dimensionless numbers tested are listed in Table II.

III. IN VITRO STUDY OF CONFINED LIQUID-IN-LIQUID INJECTION

A. Flow regimes and transition

Both the dripping and the jetting regimes may occur in the range of the control parameters indicated in Table II. The dripping regime is characterized by the periodic formation of drops at the tip of the capillary tube (Figure 3). The first phase of the formation of a drop consists of its growth up to a critical volume (Figures 3(a)–3(d)). During the detachment phase, it remains connected to the capillary tube by a liquid neck that thins out until the drop breaks up (Figures 3(e) and 3(f)). Part of the liquid neck remains attached to the capillary tip: it retracts back and a new droplet begins to grow (Figure 3(g)). This periodic process leads to the formation of constant size drops, as indicated by the small value of the coefficient of dispersion of the drop diameter,

$$\frac{\sigma(\bar{d}_d)}{\bar{d}_d} < 1.35\%.$$

The coefficient of dispersion is defined as the ratio of the standard deviation of the drop diameter $\sigma(\bar{d}_d)$ to its average value \bar{d}_d .

As the inner flow rate increases, a transition to the jetting regime occurs. It is characterized by the formation of a jet forming at the capillary tip. The jet rapidly destabilizes, leading to the formation of droplets further downstream. In this regime we observe two different patterns of drop formation depending on the inner flow rate. Above the dripping-to-jetting transition, the mechanism

TABLE II. Values of the dimensionless numbers used *in vitro*.

d_o/d_i	4.4, 6.3, 14, 20
η	10
Re_i	2–40
Re_o	200–800
We_i	0.02–10.6
Ca_o	$0.6 \times 10^{-3} - 2.9 \times 10^{-3}$
Bo	$4 \times 10^{-3} - 4 \times 10^{-2}$

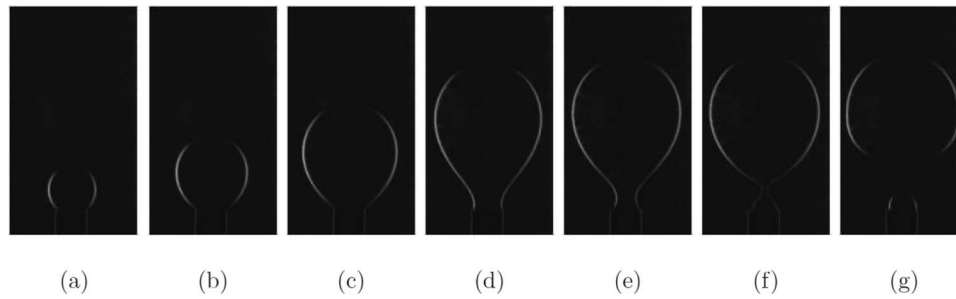


FIG. 3. Form of a drop during its formation in the dripping regime at different times t . (a) $t/t_d = 0.066$; (b) $t/t_d = 0.259$; (c) $t/t_d = 0.629$; (d) $t/t_d = 0.977$; (e) $t/t_d = 0.992$; (f) $t/t_d = 0.996$; (g) $t/t_d = 1$. $d_o/d_i = 6.3$; $We_i = 0.021$; $Ca_o = 0.0006$.

of drop formation is at first similar to that of the dripping regime (Figures 4(a)–4(c)). The only difference is that the drop breaks up at the tip of a jet and not at the extremity of the capillary tube as in the dripping regime. Occasionally, we observe the formation of satellite droplets (Figure 4(d)) as a result of the liquid thread instability. Further from the transition, the jet instability induces the periodic formation of drops that are again monodisperse.

A state diagram of the occurrence of the two regimes is shown in Figure 5 for the various values of confinement. It is plotted as a function of the Weber number of the inner flow We_i and the capillary number of the outer flow Ca_o . In practice, variations of We_i and Ca_o are obtained by varying Q_i and Q_o , respectively, since the tube diameters are set by the configuration chosen for each experiment. The dripping regime occurs for low values of We_i , when the surface tension force dominates the inertial forces of the inner flow. The experimental results show that the transition from dripping to jetting is governed by the Weber number of the inner phase. For all the results, the transition occurs around the value $We_i = 2 \pm 0.6$. No clear influence of confinement is found on the transition.

B. Drop diameter

In order to non-dimensionalize the drop diameter \bar{d}_d , the natural choice is to use the wetted diameter of the capillary tube d_w . This diameter is chosen as reference rather than d_i , since the wetting phenomenon influences the mechanism of drop formation. When the inner liquid does not wet the injection tube material, the wetted diameter d_w is equal to d_i . It is otherwise equal to the outer diameter of the injection tube. We have observed experimentally that the inner liquid presently used (silicone oil) only wets the injection tube material of the thin capillary tube (namely, polyethylene) but not that of the thicker tube (namely steel). Hence, the measured wetted diameter is

- $d_w = 0.8$ mm for the capillary tube with $d_i = 0.5$ mm;
- $d_w = 1.6$ mm for the capillary tube with $d_i = 1.6$ mm.

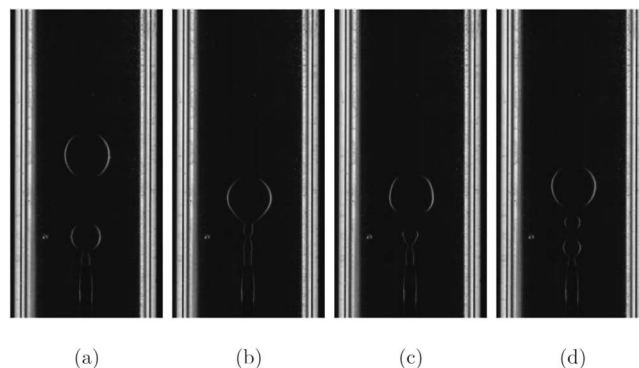


FIG. 4. Drop formation in the jetting regime for $d_o/d_i = 20$, $We_i = 3.52$, and $Ca_o = 0.0013$. (a) $t/t_d = 0.243$; (b) $t/t_d = 0.972$; (c) $t/t_d = 1$; (d) $t/t_d = 1$ with satellite drop.

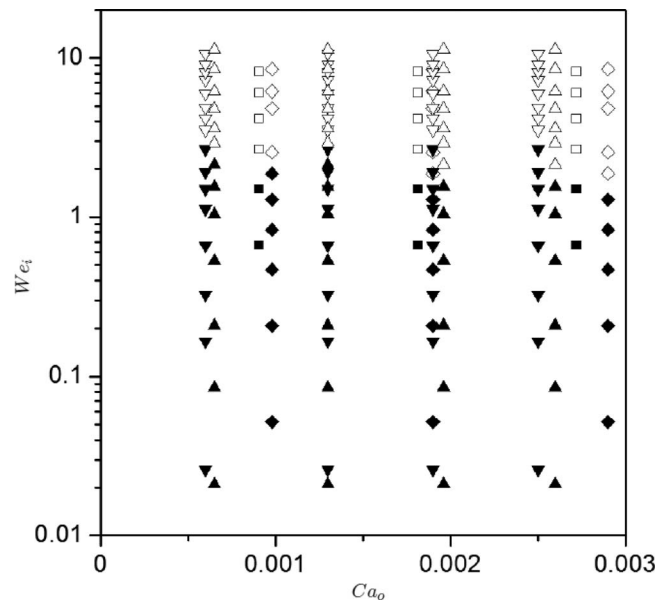


FIG. 5. State diagram showing where the dripping (solid symbols) and jetting (open symbols) regimes occur as a function of We_i and Ca_o . (∇) $d_o/d_i = 4.4$; (\triangle) $d_o/d_i = 6.3$; (\square) $d_o/d_i = 14$; (\diamond) $d_o/d_i = 20$.

The evolution of the drop size ratio $\overline{d_d}/d_w$ is shown in Figures 6(a) and 6(b) for $d_o = 10$ mm and in Figures 6(c) and 6(d) for $d_o = 7$ mm. It is plotted as a function of the inner phase Weber number We_i for different values of Ca_o .

1. Influence of the inner fluid flow

For a constant value of the outer capillary number Ca_o , the drop size ratio varies very little with We_i in the dripping regime (solid symbols in Figure 6). Its dispersion coefficient stays between 0.5% and 4.7%. The size ratio, however, decreases considerably after the dripping-to-jetting transition in the range $We_i \in [3; 6]$ to be again constant for $We_i \geq 6$. In the following, we will call the first phase of the jetting regime “transitory jetting,” and the second “established jetting.” We find that the drop size ratio reaches the constant value $\overline{d_d}/d_w \sim 2$ when $We_i \geq 6$. It is independent of the parameters We_i and Ca_o , so that it is only dictated by the wetted diameter of the capillary tube.

2. Influence of the outer fluid flow

If the inner liquid Weber number We_i mainly affects the drop size by imposing the ejection regime, a larger influence of the outer capillary number Ca_o is found especially in the dripping regime (Figure 6). This is due to the fact that it changes the friction at the liquid-liquid interface. Below the transition, the drop size ratio decreases with the outer capillary number. In the transitory jetting, the influence of Ca_o on the size ratio diminishes as We_i is increased. No influence is finally measured in the established jetting regime, when $We_i \geq 6$.

3. Influence of confinement

Another important aspect is the influence of the confinement on the drop size. One can estimate its effect by comparing Figures 6(a) and 6(b), respectively with Figures 6(c) and 6(d). It is found that the drop size ratio decreases by 15%–20%, when the outer tube diameter is reduced by 30%. In the jetting regime, no influence of confinement is, however, observed on the drop size ratio, because the drops are very small in diameter. The drop size ratio tends towards ~ 2 for larger values of We_i .

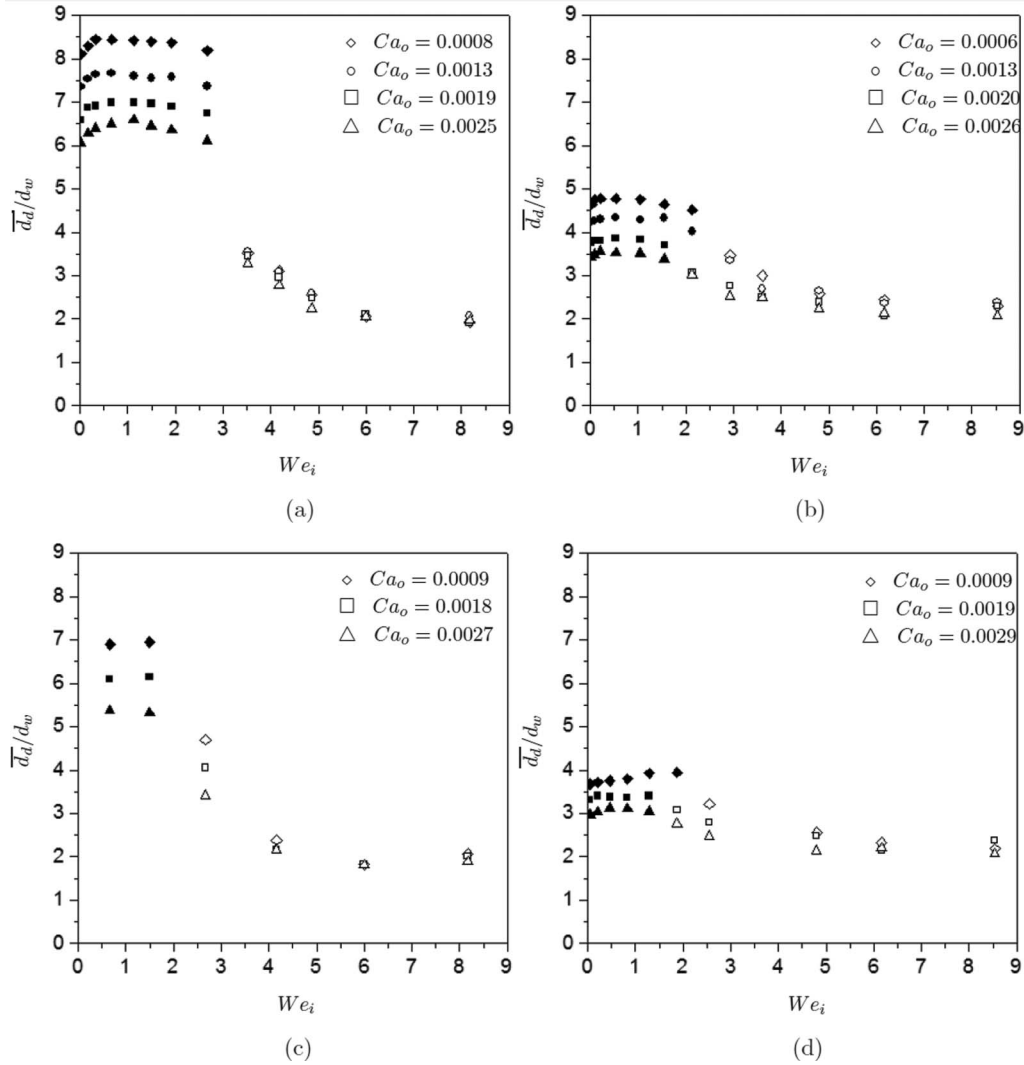


FIG. 6. Evolution of the drop size as a function of We_i and Ca_o for (a) $d_o/d_i = 20$, (b) $d_o/d_i = 6.3$, (c) $d_o/d_i = 14$, (d) $d_o/d_i = 4.4$. Solid symbols correspond to the dripping regime and open symbols to the jetting regime.

In a complementary experiment, we have measured the size of the drops obtained when injecting in an unconfined liquid at rest: the non-confined drop diameter \overline{d}_d^{NC} can then be used as reference to quantify the confinement effect. The evolution of the non-confined drop diameter \overline{d}_d^{NC} is shown in Figure 7 as a function of We_i for the same values of the diameter d_i . From the comparison of Figure 6 with Figure 7 and from the average values of $\overline{d}_d/\overline{d}_d^{NC}$ provided in Table III, one can observe that:

- The confinement effect is only negligible for the tests conducted in the large external tube ($d_o = 10$ mm) at the lowest outer capillary numbers ($Ca_o = 0.0008$ in Figure 6(a), $Ca_o = 0.0006$ in Figure 6(b)).
- Confinement otherwise has a large impact on the drop size for all the other values of outer capillary number and external tube diameter. The drop size decreases when the outer flow rate is increased or when the external tube diameter is decreased.
- Neither the external tube diameter nor the outer flow rate has an influence on the average drop size in the established jetting regime: no effect of confinement can be measured for $We_i \geq 6$, owing to the small drop size.

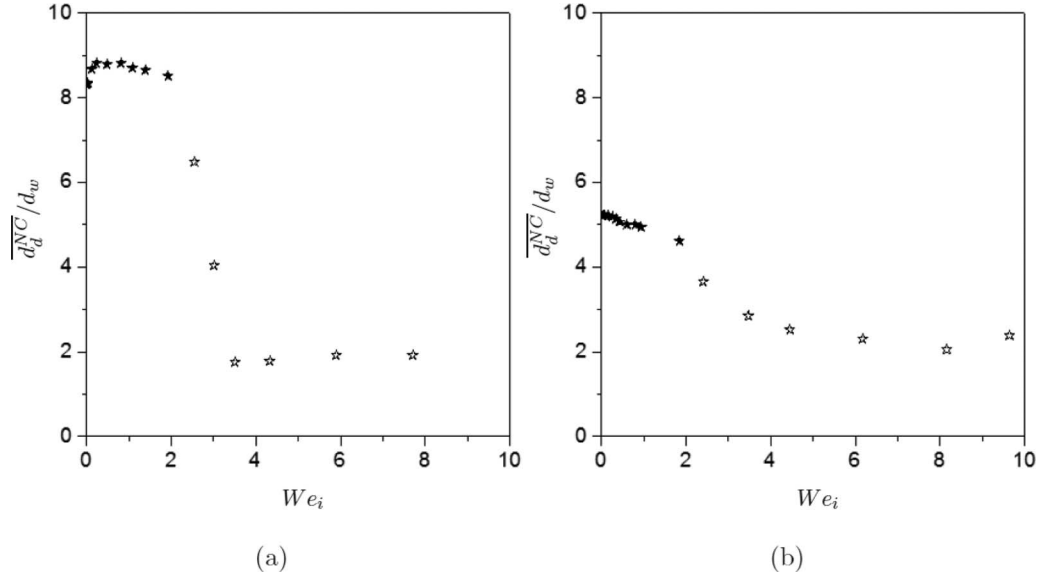


FIG. 7. Evolution of the drop size when the inner liquid is injected into a quiescent outer liquid in semi-infinite environment ($Ca_o = 0$): (a) $d_i = 0.5$ mm, (b) $d_i = 1.6$ mm. The solid symbols correspond to the dripping regime and open symbols to the jetting regime.

4. Revisiting the drop size non-dimensionalization

Previous results illustrated in Figures 6 and 7 prove that non-dimensionalizing the drop diameter by the wetted diameter of the capillary tube is the adequate non-dimensionalization for the established jetting regime. It provides an expression for the drop size ($\bar{d}_d/d_w \sim 2$) that is valid for any value of the Weber and capillary numbers. Figure 6, however, shows that the non-dimensionalization is not appropriate in the dripping regime: the diameter ratio \bar{d}_d/d_w strongly depends on the injection diameter d_i and on the outer capillary number Ca_o . A more adequate non-dimensionalization may be thought of based on the work by de Gennes *et al.*⁶² Since the drop formation, at low values of We_i and Ca_o , is mainly governed by the equilibrium between the capillary and gravitational forces, the drop size ratio depends on the Bond number as

$$\frac{\bar{d}_d}{d_w} \propto Bo^{-1/3}. \quad (1)$$

In Figure 8, we have plotted the drop size \bar{d}_d non-dimensionalized by $d_w Bo^{-1/3}$ during the dripping regime. It is interesting to see that, with the new non-dimensionalization, the drop size ratio assumes

TABLE III. Average values of \bar{d}_d/d_d^{NC} in the inner liquid ejection regimes during (a) dripping and (b) jetting for: (\blacklozenge, \diamond) $Ca_o \sim 0.0008$, (\blacksquare, \square) $Ca_o \sim 0.0019$ and ($\blacktriangle, \triangle$) $Ca_o \sim 0.0027$.

		d_o		d_o	
		7 mm	10 mm	7 mm	10 mm
d_i	0.5 mm	\blacklozenge 0.86	\blacklozenge 0.97	\diamond 0.96	\diamond 0.94
		\blacksquare 0.71	\blacksquare 0.79	\square 0.96	\square 0.96
		\blacktriangle 0.62	\blacktriangle 0.73	\triangle 0.96	\triangle 0.94
	1.6 mm	\blacklozenge 0.80	\blacklozenge 0.94	\diamond 0.99	\diamond 1.04
		\blacksquare 0.70	\blacksquare 0.78	\square 1.04	\square 1.08
		\blacktriangle 0.62	\blacktriangle 0.72	\triangle 0.95	\triangle 1.04
a) Dripping			b) Established jetting		

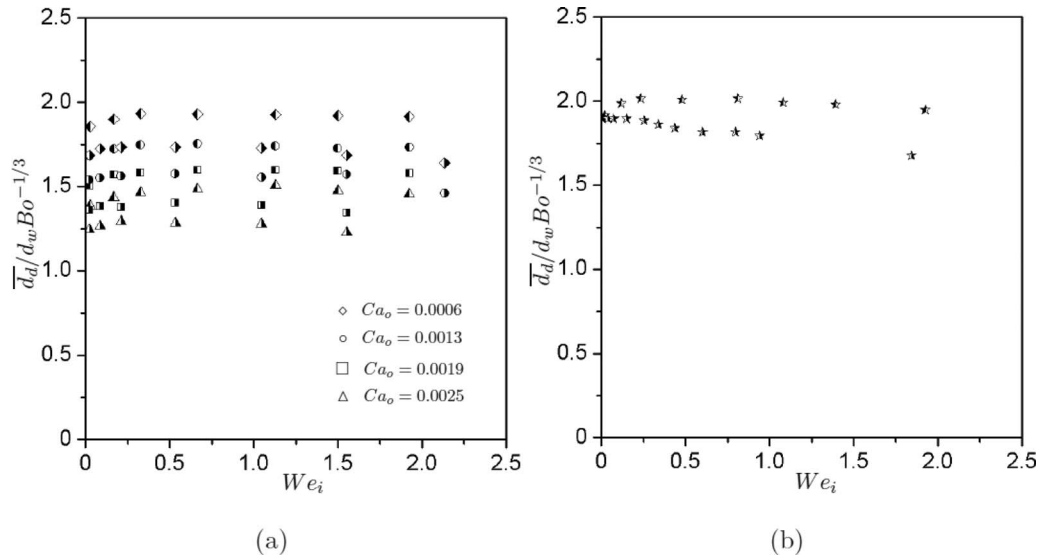


FIG. 8. Drop size \bar{d}_d non-dimensionalized by $d_w Bo^{-1/3}$ in the dripping regime for (a) $d_o = 10$ mm and (b) $d_o = \infty$ (external fluid at rest in a semi-infinite environment). Symbols half-filled on the left: $d_o/d_i = 20$. Symbols half-filled on the right: $d_o/d_i = 6.3$.

a constant value independent of the Weber number We_i :

$$\frac{\bar{d}_d}{d_w Bo^{-1/3}} = C. \quad (2)$$

The value of the constant C is close to 2 in the non-confined case (Figure 8(b)). Figure 8(a) shows that it is influenced by the tube size ratio d_o/d_i and by the outer capillary number, but it remains of order 1 in all cases ($C \sim 1.3$ – 2).

C. Drop formation time

The evolution of the mean drop formation time \bar{t}_d is shown in Figure 9 as a function of We_i and Ca_o in the case of an external tube diameter of $d_o = 10$ mm. We observe that the drop formation time decreases when We_i and/or Ca_o are increased, to become constant when $We_i \geq 6$. In the established jetting regime, the drop formation time is 2 to 3 orders of magnitude smaller than in the dripping regime.

The decrease of \bar{t}_d with We_i , measured in the dripping regime, can be predicted by the mass conservation equation

$$\frac{\pi d_d^3}{6} = Q_i t_d. \quad (3)$$

It results from the fact that the drop size remains quasi-constant with We_i . When the inner flow rate is increased, the critical volume needed for the drop to detach is reached in a shorter time lap. Equation (3) is verified precisely by most of our experimental data. The maximum value of the deviation (20%) occurs in the transitory jetting regime ($We_i \in [3; 6]$), since we have chosen to neglect the contribution of the occasionally shed small satellite droplets when estimating the drop size.

IV. THEORETICAL MODEL FOR DROP SIZE PREDICTION IN CONFINED ENVIRONMENTS

Several theoretical models^{18,29–31,63} exist to estimate the drop size in the dripping regime, but they all correspond to the formation of a drop in a semi-infinite liquid at rest. In Sec. III, we

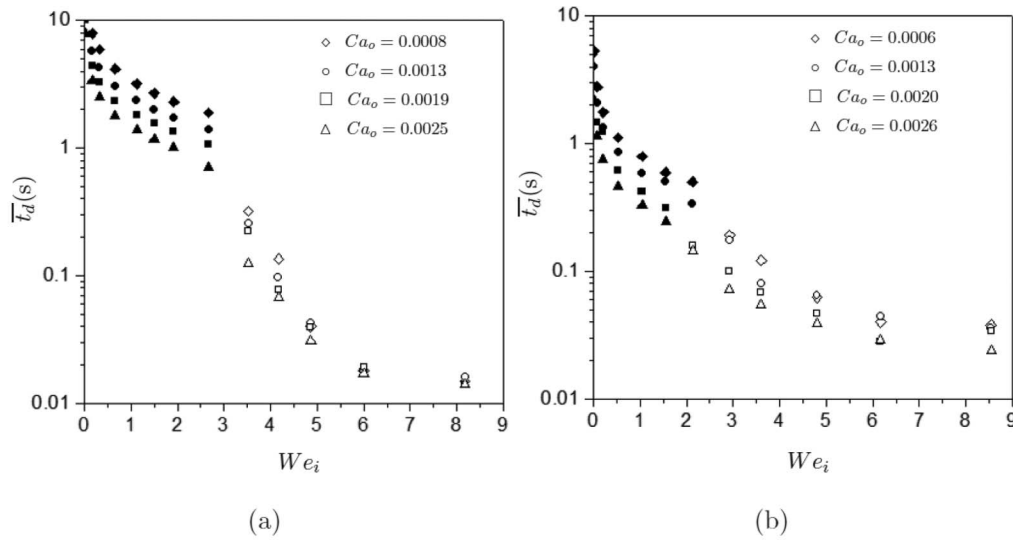


FIG. 9. Drop formation time evolution as a function of We_i and Ca_o : (a) $d_o/d_i = 20$ and (b) $d_o/d_i = 6.3$. Solid symbols correspond to the dripping regime and open symbols to the jetting regime.

have shown that both the outer flow and the presence of the outer tube play a major role in the establishment of the drop size in the case of an injection in a confined co-flow. It proves the need of a more complete theoretical model that predicts the size of the drops in the dripping regime for confined liquid-in-liquid injections. In the following, we will introduce a new theoretical model that is an extension of the model of Scheele and Meisters.²⁹ We have chosen this model as reference, as it seems to be the best compromise between accuracy and simplicity of use. In the new model we include both the influence of the confinement and of the outer phase flow on the drop size.

For a liquid injected in a denser flow in the anti-gravitational direction, two types of forces act on the drop, when it is still attached to the tip of the injection tube. If the drop rising velocity is much smaller than the outer liquid velocity, the only force that acts to keep the drop attached to the catheter tip is the interfacial tension force F_γ . The buoyancy force F_B , kinetic force F_K and drag force F_D exerted by the outer flow otherwise act to separate the drop from the tip. We apply the force balance to the drop at the end of its growing stage, i.e., just before the onset of necking,

$$F_B + F_K + F_D = F_\gamma. \quad (4)$$

The buoyancy force acting on a drop of volume V_{d1} is

$$F_B = V_{d1}g\Delta\rho, \quad (5)$$

where V_{d1} is the drop volume just before the start of the necking process, g is the gravitational acceleration, and $\Delta\rho = \rho_o - \rho_i$ is the density difference between the two liquids. The kinetic force takes into account the energy of the inner liquid exiting the injection tube transmitted to the drop in the vertical direction.²⁹ Assuming a parabolic velocity profile in the liquid leaving the nozzle, it can be written as

$$F_K = \frac{4}{3}Q_i\rho_i\overline{U}_i, \quad (6)$$

where \overline{U}_i is the average velocity of the injected liquid at the capillary tip. The interfacial tension force is

$$F_\gamma = \pi\gamma d_w. \quad (7)$$

By definition, the drag force exerted on the drop attached to the capillary tip takes the form

$$F_D = \frac{1}{2}C_D\rho_o(\Delta\overline{U})^2\frac{\pi d_{d1}^2}{4}, \quad (8)$$

where C_D is the drag coefficient, d_{d1} is the diameter of the drop of volume V_{d1} ($V_{d1} = \frac{\pi}{6}d_{d1}^3$), and $\Delta\bar{U}$ is the difference between the mean velocity of the outer fluid and the mean rising velocity of the forming drop. In the following, we will neglect the rising velocity of the drop during its formation: $\Delta\bar{U}$ is then reduced to \bar{U}_o , the mean velocity of the outer liquid. To evaluate the drag coefficient, we assume the attached drop to be a solid sphere. For a drop Reynolds number $Re_{d1} > 100$, Shaughnessy *et al.*⁶⁴ showed that the drag coefficient of a sphere flowing in a tube with circular cross section could be expressed by the correlation

$$C_D = \left[1 + 1.45 \left(\frac{d_{d1}}{d_o} \right)^{4.5} \right] C_{D\infty}. \quad (9)$$

The effect of confinement is taken into account by the size ratio d_{d1}/d_o . The drag coefficient $C_{D\infty}$ is that of a sphere placed in an infinite environment under an outer flow with Reynolds number Re_{d1} . Many empirical expressions of $C_{D\infty}$ may be found in the literature for a wide range of Re_{d1} values (a summary is provided by Almedeij⁶⁵). We will use the expression given by Schiller *et al.*,⁶⁶ which is applicable within the range $2 < Re_{d1} < 800$:

$$C_{D\infty} = \frac{24}{Re_{d1}} (1 + 0.15 Re_{d1}^{0.687}). \quad (10)$$

The force balance (Eq. (4)) provides an expression of the drop volume V_{d1} , if one divides both sides of the equation by $g\Delta\rho$. Replacing the forces by their expressions (Eqs. (5)–(10)), one finds an implicit equation for d_{d1} :

$$\frac{\pi d_{d1}^3}{6} = \frac{\pi \gamma d_w}{g \Delta \rho} - \frac{4 Q_i \rho_i \bar{U}_i}{3 g \Delta \rho} - \frac{3 \pi \mu_o d_{d1} \bar{U}_o}{g \Delta \rho} \times \left(1 + 1.45 \left(\frac{d_{d1}}{d_o} \right)^{4.5} \right) \times \left(1 + 0.15 \left(\frac{\rho_o \bar{U}_o d_{d1}}{\mu_o} \right)^{0.687} \right). \quad (11)$$

Equation (11) is solved by iterations. A first guess is obtained assuming $C_D = 1$, which corresponds to a rigid sphere in an infinite environment under an outer flow with Reynolds number $Re_{d1} = 10^2$ (Shaughnessy *et al.*,⁶⁴ Roos and Willmarth⁶⁷). A solution for d_{d1} is typically obtained in less than 20 iterations for a convergence criteria of 10^{-5} m.

In order to obtain the final volume of the detaching drop, one must take into account the additional volume V_{d2} that enters the drop during the necking process (second stage in the drop formation mechanism). Scheele and Meister²⁹ proposed an empirical correlation for this additional drop volume

$$V_{d2} = K \left(\frac{Q_i^2 d_w^2 \rho_i \gamma}{g^2 (\Delta \rho)^2} \right)^{1/3}, \quad (12)$$

in which K is obtained experimentally. To estimate K , we have measured the drop necking time t_N in a series of experiments, in which the inner and outer flow rates were varied along with the capillary tube diameter. From the values of t_N , we have calculated the experimental additional volume V_{d2}^{exp} that enters the drop during the necking process as

$$V_{d2}^{exp} = Q_i \cdot t_N. \quad (13)$$

Figure 10(a) shows the variation of the ratio $V_{d2}^{exp} / \left(\frac{Q_i^2 d_w^2 \rho_i \gamma}{g^2 (\Delta \rho)^2} \right)^{1/3}$, i.e., K , with the outer capillary number Ca_o and inner Weber number We_i . A dependency of K on Ca_o , We_i and d_i is observed: lower values of K are found when increasing Ca_o and We_i or decreasing d_i . In order to get the optimal value of K , we have determined the relation of proportionality between V_{d2}^{exp} and $\left(\frac{Q_i^2 d_w^2 \rho_i \gamma}{g^2 (\Delta \rho)^2} \right)^{1/3}$ that best fits all the data points (Figure 10(b)). For our liquid–liquid system, we find $K \simeq 0.5$.

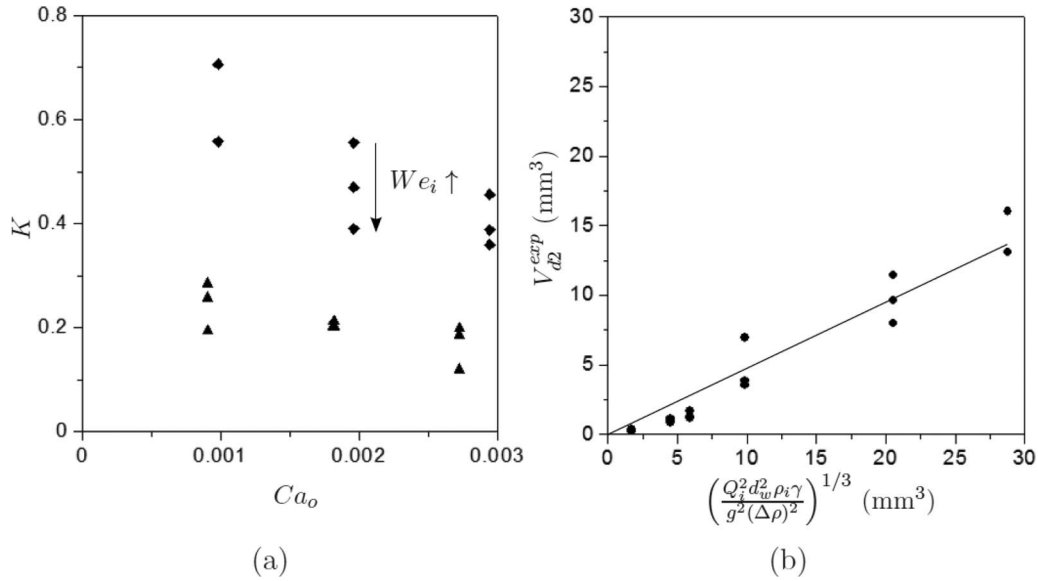


FIG. 10. (a) Evolution of K as a function of Ca_o and We_i for $d_i = 0.5$ mm (▲) and $d_i = 1.6$ mm (◆). The inner Weber numbers tested are $We_i = 0.04, 0.5$ and 1.5 . (b) Estimation of the optimal value of K corresponding to the relation of proportionality between V_{d2}^{exp} and $\left(\frac{Q_i^2 d_w^2 \rho_i \gamma}{g^2 (\Delta \rho)^2}\right)^{1/3}$ (continuous line) that best fits the data points.

The final volume of the detached drop is given by

$$\frac{\pi d_d^3}{6} = F_{HB} (V_{d1} + V_{d2}). \quad (14)$$

The coefficient F_{HB} is the correction factor introduced by Harkins and Brown⁶⁸ that takes into account the fraction of the growing drop that remains attached to the tip of the injection tube after the drop breakoff. This coefficient can be estimated using either Figure 3 of Scheele and Meister²⁹ or the correlations of Clift *et al.*⁶⁹ (page 331).

The drop diameter d_d is compared with the experimental results in Figure 11 for the two injection tubes and an external tube diameter $d_o = 10$ mm. We calculated an average deviation between model and experiments of 10%, the deviation varying from 0.2% to 29%. Good agreement with the experimental results is found also when an external tube of a smaller diameter ($d_o = 7$ mm) is used (data not shown). As Figure 11 shows, the model has the tendency to underestimate the drop size when the inner liquid flow rate is increased. The model assumptions and the empirical correlations used to derive an estimation of the drop diameter are most probably the cause of the discrepancy. For instance we have neglected the drop rising velocity during its formation at the capillary tip. The drop rising velocity has the effect of reducing the relative velocity in the drag force estimation: taking it into account would have probably reduced the discrepancy. We have also considered the drop to be a solid sphere: it enabled us to have a simple approximation of the drag force but introduced a limitation on the model accuracy. Still the error remains overall reasonably low. It must be underlined that it is of the same order of magnitude as that of Scheele and Meister's model.²⁹

V. IMPLICATION FOR VEIN EMBOLIZATION BY GLUE INJECTION

In the present study, we have investigated the injection of a liquid phase in a confined liquid system with the objective to better understand the physical phenomena that are at stake during the embolization of veins by glue injection. The study has concentrated on the specific case of PVE. But the results are transferrable to other clinical uses of vein embolization, as they cover a larger range of parameters. The external flow has been modeled as steady, since MRI measurements have proven

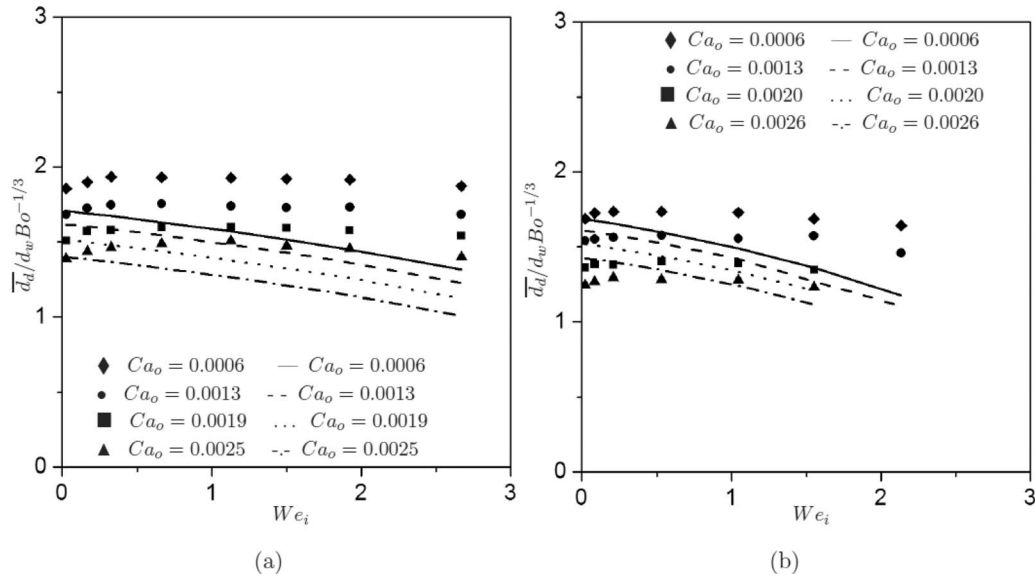


FIG. 11. Comparison of the drop diameter predicted by the theoretical model with the experimental results for (a) $d_o/d_i = 20$ and (b) $d_o/d_i = 6.3$.

the very low pulsatility of the blood flow in the portal vein.⁷⁰ Assuming steady blood flow is valid for any vein embolization case. More investigations on the influence of pulsatility on the injection dynamics are, however, needed, before applying the present results to arterial embolization.

In the first part of the study, we have reproduced *in vitro* the physiological conditions encountered during PVE and simulated the procedure in a series of experiments. We have looked at the influence of confinement and blood co-flow: we have changed the confinement ratio, as well as the Weber number of the inner flow We_i and capillary number of the outer flow Ca_o . All the values of the non-dimensional parameters indicated in Table II have been chosen to ascertain that the *in vitro* experiments are in similarity with the physiological case of PVE. When one compares the *in vitro* values tested (Table II) with the typical ranges of values that are encountered during PVE (Table IV), one can see that the similarity has been respected for all the non-dimensional numbers, except the outer capillary number. The latter, too small by one order of magnitude in the *in vitro* simulation, could not be matched: we never found two immiscible fluids with exactly the same properties as the *in vivo* fluid couple (liquid glue–blood). We have opted to guarantee identical Reynolds and inner Weber number and conduct the experiment with a slightly smaller outer capillary number, since the latter is anyway infinitely small compared to unity.

TABLE IV. *In vivo* values of the dimensionless numbers during portal vein embolization. They are calculated from clinical measurements conducted by the Departments of Radiology and Imaging & Biophysics from the CHU Amiens (unpublished data, but more information on the methodology may be found in Yzet *et al.*⁷⁰).

<i>In vivo</i>	
d_o/d_i	4.4, 6.3, 14, 20
μ_i/μ_o	1–8
Re_i	≤ 15
Re_o	200–600
We_i	≤ 2
Ca_o	$28 \times 10^{-3} - 50 \times 10^{-3}$
Bo	$\leq 6 \times 10^{-2}$

From the experimental results, one can conclude that, in the case of PVE, the injected liquid glue forms drops either at the tip of the capillary tube (dripping regime) or downstream of a liquid jet (jetting regime). The parameter that governs the dripping-to-jetting transition is the Weber number of the injected liquid We_i : no influence of confinement has been found for the transition. For low values of We_i ($We_i \leq \mathcal{O}(1)$), surface tension dominates over the inertial forces of the inner flow and drops are formed at the tip of the injection tube. Once surface tension no longer dominates ($We_i \geq \mathcal{O}(1)$), the forming drop is convected downstream, favoring the formation of a liquid jet. On average, the transition to the jetting regime is observed for $We_i = 2 \pm 0.6$ (i.e., $\mathcal{O}(1)$). Our results correlate perfectly with those obtained by Utada *et al.*⁶⁰ in a microfluidic co-injector for very large confinement ratios d_o/d_i . Utada *et al.*⁶⁰ also found that another type of transition to the jetting regime is possible for $Ca_o \geq \mathcal{O}(1)$, when the viscous drag exerted by the outer liquid flow dominates surface tension. But owing to the small values of Ca_o (Table IV), such a transition cannot occur during PVE.

In the physiological conditions of glue embolization, the injection is typically performed at Weber numbers $We_i \leq 2$ (Table IV). Glue embolization is, therefore, performed mainly in the dripping regime. In this regime, the drop size is strongly influenced by the capillary number of the blood flow Ca_o and by confinement (Figure 6). It, however, remains almost constant regardless of the value of the Weber number of the injected fluid We_i . One can conclude that:

- The drop detaches from the capillary tip, when the buoyancy and viscous drag forces overpass surface tension.
- The inertial force of the injected glue (and therefore We_i) only marginally influences the drop critical volume at detachment. It only affects the drop formation time t_d , as it determines how quickly the drop reaches its critical volume.
- The drop size is strongly conditioned by the diameter of the outer tube. The confinement effect is clearly shown by the average values of $\overline{d_d}/\overline{d_d}^{NC}$ in Table III. The only case, where hardly no confinement effect is measured, is for the lowest value of blood flow ($Ca_o \sim 0.0008$) and $d_o = 10$ mm. Confinement can otherwise never be neglected in the dripping regime.

The *in vivo* parameter values indicated in Table IV show that PVE may also occur at the beginning of the jetting regime, in the transitory jetting regime. The main differences with the dripping regime is that the drops break up at the tip of a (short) jet and no longer at the capillary tip; they are shed aperiodically and have a size dispersion, because of the jet instability. This subregime is characterized by smaller drop sizes, but a much higher frequency of shedding than in dripping. The influence of confinement is thus less pronounced. The drop size/formation time decreases when We_i and/or Ca_o are increased, but the influence of the parameters fades out, as one approaches the established jetting regime. For $We_i \geq 6$, neither the flow parameters nor confinement affects the size of the small drops: it solely depends on the diameter of the jet, which is set by the catheter tube diameter. Injecting in the established jetting regime may seem like a great solution to embolize small distal vessels, as small calibrated glue drops are produced. But reaching such high values of We_i may be difficult clinically: interventional radiologists would have to choose a very small injection tube diameter d_i and a high injection flow rate Q_i . If the established jetting regime seems out of reach, interventional radiologists can still exploit the possibility of ejecting glue in either of the two regimes: drops of different sizes can thus be generated, which offers the possibility to adapt the drop size depending on the vessel diameter.

To complete the experimental characterization of the liquid glue ejection, we have developed a new theoretical model that predicts the drop size in the dripping regime. The model, based on the work by Scheele and Meister,²⁹ takes into account the confinement and external flow effects. The drop diameter is obtained writing the force balance just before necking starts. To determine the viscous forces, we have assumed the drop to be a solid sphere. Despite the crudeness of the assumption, the new model proves to be a good compromise between accuracy and simplicity of use: the implicit equation (11) rapidly converges towards the solution. Since the model takes into account all the controlling parameters involved in a typical liquid–liquid system, it will be of use for the interventional radiologists to choose the appropriate size of drops in order to optimize the vessel occlusion.

Theoretical models predicting the drop size have also been developed for the established jetting regime (although not in the transitory jetting subregime). Existing models can directly be applied to the case of glue embolization, since we have proven that the effect of confinement is negligible in the fully established jetting regime (Table III). The drop size value may, for instance, be obtained from the model of Kitamura *et al.*,⁴⁴ to cite one among others. Even if interventional radiologists may never eject glue in this subregime, knowing the asymptotic drop size may still prove to be useful.

It must finally be stressed out that all the present results will only apply to the physiological use of glue embolization, so long as the effects of polymerization do not perturb much the injection dynamics. We have conducted a preliminary study on the injection of mixtures of glue with lipiodol in a blood substitute having the same ionic content as blood. We have found that the influence of polymerization is negligible for low concentrations in glue in the injected mixture (e.g. 25% of glue and 75% of lipiodol). The results of the present study should therefore be applicable to the clinical use of embolization, as long as the glue concentration remains low. Still, a complete study of the effects of glue polymerization is needed to quantify the domain of validity of the present results.

ACKNOWLEDGMENTS

This work was supported by the Conseil Régional de Picardie (EMBOLOTHERAPIE grant) and by the French Ministère de la Recherche (Ph.D. scholarship of M.-C. Sandulache).

- ¹ J. S. Pollak and R. I. White, "The use of cyanoacrylate adhesives in peripheral embolization," *J. Vasc. Interv. Radiol.* **12**(8), 907–913 (2001).
- ² S. C. Kramer, J. Gorich, N. Rilinger, M. Siech, A. J. Aschoff, J. Vogel, and H. J. Brambs, "Embolization for gastrointestinal hemorrhages," *Eur. Radiol.* **10**(5), 802–805 (1991).
- ³ G. M. Debrun, V. Aletich, J. Ausman, F. Charbel, and M. Dujovny, "Embolization of the nidus of brain arteriovenous malformations with n-butyl cyanoacrylate," *Neurosurgery* **40**(1), 112–121 (1997).
- ⁴ R. C. Wallace, R. A. Flom, M. H. Khayata, B. L. Dean, J. McKenzie, J. C. Rand, N. A. Obuchowski, R. C. Zepp, J. M. Zabramski, and R. R. F. Spetzler, "The safety and effectiveness of brain arteriovenous malformation embolization using acrylic and particles: The experiences of a single institution," *Neurosurgery* **37**(4), 606–618 (1995).
- ⁵ E. Abdalla, C. Barnett, D. Doherty, S. Curley, and J. Vauthey, "Extended hepatectomy in patients with hepatobiliary malignancies with and without preoperative portal vein embolization," *Arch. Surg. (Chicago)* **137**(6), 675–681 (2002).
- ⁶ D. Madoff, E. Abdalla, and J. Vauthey, "Portal vein embolization in preparation for major hepatic resection: Evolution of a new standard of care," *J. Vasc. Interv. Radiol.* **16**(6), 779–790 (2005).
- ⁷ M. Shoup, M. Gonen, M. D'Angelica, W. Jarnagin, R. DeMatteo, L. Schwartz, S. Tuorto, L. Blumgart, and Y. Fong, "Volumetric analysis predicts hepatic dysfunction in patients undergoing major liver resection," *J. Gastrointest Surg.* **7**(3), 325–330 (2003).
- ⁸ J. Vauthey, A. Chaoui, K. Do, M. Bilimoria, M. Fenstermacher, C. Charnsangavej, M. Hicks, G. Alsfasser, G. Lauwers, I. Hawkins, and J. Caridi, "Standardized measurement of the future liver remnant prior to extended liver resection: Methodology and clinical associations," *Surgery* **127**(5), 512–519 (2000).
- ⁹ O. Farges, J. Belghiti, R. Kianmanesh, J. M. Regimbeau, R. Santoro, V. Vilgrain, A. Denys, and A. Sauvanet, "Portal vein embolization before right hepatectomy. Prospective clinical trial," *Ann. Surg.* **237**(2), 208–218 (2003).
- ¹⁰ S. Kull, I. Martinelli, E. Briganti, P. Losi, D. Spiller, S. Tonlorenzi, and G. Soldani, "Glubran2 surgical glue: *In vitro* evaluation of adhesive and mechanical properties," *J. Surg. Res.* **157**, e15–e21 (2009).
- ¹¹ R. Rosen and S. Contractor, "The use of cyanoacrylate adhesives in the management of congenital vascular malformations," *Semin Interv Radiol.* **21**(1), 59–66 (2004).
- ¹² A. H. White and F. T. Smith, "Wall shape effects on multiphase flow in channel," *Theor. Comput. Fluid Dyn.* **26**, 339–360 (2012).
- ¹³ A. White, "Mathematical modelling of the embolization process in the treatment of arteriovenous malformations," Ph.D. dissertation (University of London, 2008).
- ¹⁴ J. Plateau, "Recherches expérimentales et théoriques sur les figures d'équilibre d'une masse liquide sans pesanteur," *Acad. Sci. Bruxelles Mem.* **23**, 5 (1849).
- ¹⁵ L. Rayleigh, "On the instability of jets," *Proc. London Math. Soc.* **s1-10**, 4–13 (1878).
- ¹⁶ H. A. Stone, "Dynamics of drop deformation and breakup in viscous fluids," *Annu. Rev. Fluid Mech.* **26**, 65–102 (1994).
- ¹⁷ V. Cristini and Y.-C. Tan, "Theory and numerical simulation of droplet dynamics in complex flows: A review," *Lab Chip* **4**, 257–264 (2004).
- ¹⁸ C. B. Hayworth and R. E. Treybal, "Drop formation in two-liquid-phase systems," *Ind. Eng. Chem.* **42**(6), 1174–1181 (1950).
- ¹⁹ K. Fujinawa, T. Maruyama, and Y. Nakaike, "Drop formation in liquid-liquid systems," *J. Chem. Eng. (Japan)* **21**, 194–200 (1957).

- ²⁰ R. Scardovelli and S. Zaleski, "Direct numerical simulation of free-surface and interfacial flow," *Annu. Rev. Fluid Mech.* **31**, 567–603 (1999).
- ²¹ H. A. Stone and L. G. Leal, "Relaxation and breakup of an initially extended drop in an otherwise quiescent fluid," *J. Fluid Mech.* **198**, 399–427 (1989).
- ²² M. Rayner, G. Trägårdh, C. Trägårdh, and P. Dejmeek, "Using the surface evolver to model droplet formation processes in membrane emulsification," *J. Colloid Interface Sci.* **279**, 175–185 (2004).
- ²³ G. Tryggvason, B. Bunner, A. Esmaeeli, D. Juric, N. Al-Rawahi, W. Tauber, J. Han, S. Nas, and Y.-J. Jan, "A front-tracking method for the computations of multiphase flow," *J. Comput. Phys.* **169**, 708–759 (2001).
- ²⁴ J. Richards, A. Beris, and A. Lenhoff, "Drop formation in liquid-liquid systems before and after jetting," *Phys. Fluids* **7**, 2617–2630 (1995).
- ²⁵ D. Gueyffier, J. Li, A. Nadim, R. Scardovelli, and S. Zaleski, "Volume-of-fluid interface tracking with smoothed surface stress methods for three-dimensional flows," *J. Comput. Phys.* **152**, 423–456 (1999).
- ²⁶ X. Yang, J. J. Feng, C. Liu, and J. Shen, "Numerical simulations of jet pinching-off and drop formation using an energetic variational phase-field method," *J. Comput. Phys. Fluids* **218**, 417–428 (2006).
- ²⁷ R. Nourgaliev, T. Dinh, T. Theofanous, and D. Joseph, "The lattice Boltzmann equation method: Theoretical interpretation, numerics and implications," *Int. J. Multiphase Flow* **29**, 117–169 (2003).
- ²⁸ E. N. Rao, R. Kumar, and N. Kuloor, "Drop formation studies in liquid-liquid systems," *Chem. Eng. Sci.* **21**(10), 867–880 (1966).
- ²⁹ G. Scheele and B. Meister, "Drop formation at low velocities in liquid-liquid systems: Part I – Prediction of drop volume," *AIChE J.* **14**, 9–15 (1968).
- ³⁰ L. de Chazal and J. Ryan, "Formation of organic drops in water," *AIChE J.* **17**, 1226–1229 (1971).
- ³¹ J. Izard, "Prediction of drop volumes in liquid-liquid systems," *AIChE J.* **18**, 634–638 (1972).
- ³² D. F. Zhang and H. A. Stone, "Drop formation in viscous flows at a vertical capillary tube," *Phys. Fluids* **9**(8), 2234–2242 (1997).
- ³³ X. Zhang, "Dynamics of drop formation in viscous flows," *Chem. Eng. Sci.* **54**(12), 1759–1774 (1999).
- ³⁴ I. B. Bazhlekov, P. D. Anderson, and H. E. H. Meijer, "Nonsingular boundary integral method for deformable drops in viscous flows," *Phys. Fluids* **16**, 1064 (2004).
- ³⁵ T. Thorsen, R. W. Roberts, F. H. Arnold, and S. R. Quake, "Dynamic pattern formation in a vesicle-generating microfluidic device," *Phys. Rev. Lett.* **86**, 4163–4166 (2001).
- ³⁶ S. L. Anna, N. Bontoux, and H. A. Stone, "Formation of dispersions using "flow focusing" in microchannels," *Appl. Phys. Lett.* **82**, 364–366 (2003).
- ³⁷ D. R. Link, S. L. Anna, D. A. Weitz, and H. A. Stone, "Geometrically mediated breakup of drops in microfluidic devices," *Phys. Rev. Lett.* **92**(5), 054503 (2004).
- ³⁸ P. Garstecki, M. J. Fuerstman, H. A. Stone, and G. M. Whitesides, "Formation of droplets and bubbles in a microfluidic T-junction-scaling and mechanism of break-up," *Lab Chip* **6**, 437–446 (2006).
- ³⁹ A. Marin, F. Campo-Cortesa, and J. Gordillo, "Generation of micron-sized drops and bubbles through viscous co-flows," *Colloids Surf., A* **344**, 2–7 (2009).
- ⁴⁰ C. N. Baroud, F. Gallaire, and R. Dangla, "Dynamics of microfluidic droplets," *Lab Chip* **10**, 2032–2045 (2010).
- ⁴¹ C. Zhou, P. Yue, and J. Feng, "Formation of simple and compound drops in microfluidic devices," *Phys. Fluids* **18**, 092105 (2006).
- ⁴² S. van der Graaf, T. Nisisako, C. G. P. H. Schroën, R. G. M. van der Sman, and R. M. Boom, "Lattice Boltzmann simulations of droplet formation in a T-shaped microchannel," *Langmuir* **22**, 4144–4152 (2006).
- ⁴³ P. Umbanhowar, V. Prasad, and D. Weitz, "Monodisperse emulsion generation via drop break off in a coflowing stream," *Langmuir* **16**(2), 347–351 (2000).
- ⁴⁴ Y. Kitamura, H. Mishima, and T. Takahashi, "Stability of jets in liquid-liquid systems," *Can. J. Chem. Eng.* **60**, 723–731 (1982).
- ⁴⁵ S. Homma, J. Koga, S. Matsumoto, M. Song, and G. Tryggvason, "Breakup mode of an axisymmetric liquid jet injected into another immiscible liquid," *Chem. Eng. Sci.* **61**, 3986–3996 (2006).
- ⁴⁶ E. Tyler, "Instability of liquid jets," *Philos. Mag.* **16**, 504–518 (1933).
- ⁴⁷ S. Tomotika, "On the stability of a cylindrical thread of a viscous liquid surrounded by another viscous liquid," *Proc. R. Soc. Lond., Ser. A, Math. Phys. Sci.* **150**, 322–337 (1935).
- ⁴⁸ B. Meister and G. Scheele, "Generalized solution of the Tomotika stability analysis for a cylindrical jet," *AIChE J.* **13**, 682–688 (1967).
- ⁴⁹ B. Meister and G. Scheele, "Prediction of jet length in immiscible liquid systems," *AIChE J.* **15**(5), 689–699 (1969).
- ⁵⁰ B. Meister and G. Scheele, "Drop formation from cylindrical jets in immiscible liquid systems," *AIChE J.* **15**(5), 700–706 (1969).
- ⁵¹ A. Bright, "Minimum drop volume in liquid jet breakup," *Chem. Eng. Res. Des.* **63**(1), 59–66 (1985).
- ⁵² T. Das, "Prediction of jet breakup length in liquid-liquid systems using the Rayleigh-Tomotika analysis," *Atomization Sprays* **7**, 549–559 (1997).
- ⁵³ P. Guillot, A. Colin, A. S. Utada, and A. Ajdari, "Stability of a jet in confined pressure-driven biphasic flows at low Reynolds numbers," *Phys. Rev. Lett.* **99**, 104502 (2007).
- ⁵⁴ P. Guillot, A. Ajdarib, J. Goyona, M. Joanicota, and A. Colin, "Droplets and jets in microfluidic devices," *C. R. Chimie* **12**(1–2), 247–257 (2009).
- ⁵⁵ A. Utada, A. Fernandez-Nieves, J. Gordillo, and D. Weitz, "Absolute instability of a liquid jet in a co-flowing stream," *Phys. Rev. Lett.* **100**(1), 014502 (2008).
- ⁵⁶ C. Clanet and J. C. Lasheras, "Transition from dripping to jetting," *J. Fluid Mech.* **383**, 307–326 (1999).
- ⁵⁷ B. Ambravaneswaran, H. J. Subramani, S. D. Phillips, and O. A. Basaran, "Dripping-jetting transitions in a dripping faucet," *Phys. Rev. Lett.* **93**, 034501 (2004).

- ⁵⁸ A. Sevilla, J. M. Gordillo, and C. Martnez-Bazn, "Transition from bubbling to jetting in a coaxial air-water jet," *Phys. Fluids* **17**, 018105 (2005).
- ⁵⁹ C. Cramer, P. Fischer, and E. Windhab, "Drop formation in a co-flowing fluid," *Chem. Eng. Sci.* **52**, 3045–3058 (2004).
- ⁶⁰ A. Utada, A. Fernandez-Nieves, H. Stone, and D. Weitz, "Dripping to jetting transitions in co-flowing liquid streams," *Phys. Rev. Lett.* **99**(9), 094502 (2007).
- ⁶¹ E. Castro-Hernandez, V. Gundabala, A. Fernandez-Nieves, and J. Gordillo, "Scaling the drop size in co-flow experiments," *New J. Phys.* **11**, 075021 (2009).
- ⁶² P. de Gennes, F. Brochard-Wyart, and D. Quéré, *Capillarity and Wetting Phenomena: Drops, Bubbles, Pearls, Waves* (Springer, New York, 2004).
- ⁶³ H. R. Null and H. F. Johnson, "Drop formation in liquid-liquid systems from single nozzles," *AIChE J.* **4**(3), 273–281 (1958).
- ⁶⁴ E. Shaughnessy, I. Katz, and J. Schaffer, *Introduction to Fluid Mechanics* (Oxford University Press, New York, 2005), p. 920.
- ⁶⁵ J. Almedeij, "Coefficient of flow around a sphere: Matching asymptotically the wide trend," *Powder Technol.* **186**, 218–223 (2008).
- ⁶⁶ L. Schiller and A. Nauman, "Über die grundlegenden Berechnungen bei der Schwerkraftaufbereitung," *Z. Ver. Dtsch. Ing.* **77**, 318–320 (1933).
- ⁶⁷ F. Roos and W. Willmarth, "Some experimental results on sphere and disk drag," *AIAA J.* **9**(2), 285–291 (1971).
- ⁶⁸ W. Harkins and F. Brown, "The determination of surface tension (free surface energy) and the weight of falling drops: The surface tension of water and benzene by the capillary height method," *J. Am. Chem. Soc.* **41**, 499–524 (1919).
- ⁶⁹ R. Clift, J. Grace, and M. Weber, *Bubbles, Drops, and Particles* (Academic, New York, 1978), p. 331.
- ⁷⁰ T. Yzet, R. Bouzerar, O. Balédent, C. Renard, D. M. Lumbala, E. Nguyen-Khacc, J.-M. Regimbeaud, H. Deramond, and M.-E. Meyer, "Dynamic measurements of total hepatic blood flow with phase contrast MRI," *Eur. J. Radiol.* **73**, 119–124 (2010).